HHS Public Access

Author manuscript

Nat Neurosci. Author manuscript; available in PMC 2010 July 01.

Published in final edited form as:

Nat Neurosci. 2010 January ; 13(1): 53–59. doi:10.1038/nn.2444.

Spike integration and cellular memory in a rhythmic network from Na^+/K^+ pump current dynamics

Stefan R. Pulver and **Leslie C. Griffith**

Brandeis University, Department of Biology, National Center of Behavioral Genomics and Volen Center for Complex Systems, Waltham, MA 02454-9110

Abstract

The output of a neural circuit results from an interaction between the intrinsic properties of neurons within the circuit and the features of the synaptic connections between them. The plasticity of intrinsic properties has been primarily attributed to modification of ion channel function and/or number. In this study, we demonstrate a mechanism for intrinsic plasticity in rhythmically active *Drosophila* neurons that is not conductance-based. Larval motor neurons show a long lasting sodium-dependent afterhyperpolarization (AHP) following bursts of action potentials that is mediated by the electrogenic activity of Na^+/K^+ ATPase. This AHP persists for multiple seconds following volleys of action potentials and is able to function as a pattern-insensitive integrator of spike number that is independent of external calcium. This current also interacts with endogenous *Shal* K^+ conductances to modulate spike timing for multiple seconds following rhythmic activity, providing a cellular memory of network activity on a behaviorally relevant time scale.

Keywords

Na^+/K^+ ATPase; after-hyperpolarization; neuronal plasticity; spike counter; central pattern generators; rhythmic network

INTRODUCTION

Activity integrators in the nervous system are critical for acutely sculpting neuronal responses and, in the longer term, for engaging homeostatic processes. Ca^{2+} is a ubiquitously used second messenger in neurons and it has been shown to be involved in both regulation of synaptic strength [1] and in regulation of intrinsic properties [2–4]. Ca^+-based integrators of near-term activity, however, have several limitations. First, they operate on fast time scales (msec to hundreds of msec) due to time constant of Ca^{2+} clearance [5]. More importantly, however, Ca^{2+} levels are not necessarily linear with spike number due to the kinetics of voltage-gated Ca^{2+} channels [6] and cellular Ca^{2+} buffers [7, 8]. These kinetic

Correspondence to: Leslie C. Griffith.

Author contributions: S.R.P. and L.C.G. designed experiments. S.R.P. performed experiments and analyzed data. S.R.P. and L.C.G. wrote the paper together.

constraints complicate linear integration of synaptic activity over longer (sec to min) time scales by Ca^{2+} sensors.

While Na^+ is not widely considered to be a second messenger, its intracellular level is directly linked with neuronal spiking. Indeed, previous work demonstrates that neuronal activity in small neurons can generate large and long lasting changes in intracellular Na^+ [9], [10]. This suggests that activity sensors tuned to intracellular Na^+ could be potentially useful as regulators of neuronal function. Such sensors could bridge the temporal gap between the signaling by Ca^{2+} of fast (single spike or burst) and slow (transcriptional) events allowing the neuron to be tuned in response to synaptic activity that occurs over seconds to minutes. This timescale is particularly relevant to rhythmically active networks such as those controlling respiration[11] locomotion[12], feeding [13] or swimming [14] which typically fire in the 0.5–2 Hz range.

The *Drosophila* third instar larval locomotor circuit provides an ideal system in which to investigate the mechanisms of plasticity on this timescale. Forward movement in larvae is generated by waves of body wall muscle contractions that are controlled by a segmentally coordinated central pattern generator (CPG). The output of the CPG can be monitored by observing stride frequency (ca. 1Hz; [15]) in intact animals or by recording bursting activity (ca. 0.1 Hz; [16], [17]) from motor nerves or muscles in a dissected body wall preparation.

To investigate cellular processes that might mediate plasticity on this time scale, we recorded from motor neurons and identified an afterhyperpolarization (AHP) following bursts of action potentials that lasted for multiple seconds. Using a combination of electrophysiological assays, pharmacology, and genetics we show that the AHP is mediated by electrogenic activity of the Na^+/K^+ ATPase, instead of a change in membrane conductance. This pump current interacts with other intrinsic conductances during behaviorally relevant rhythmic activity and can act both as a integrator of spike number (regardless of activity pattern) and as a Ca^{2+}-independent intrinsic short-term memory mechanism in larval motor neurons.

RESULTS

Earlier work characterized the basic electrophysiological features and projection patterns of 5 segmentally repeating, dorsal motor neurons in the ventral ganglion of 3rd instar larvae [18]. These motor neurons fire high frequency rhythmic bursts during the peristaltic body waves that drive larval locomotion [16]. In other rhythmic systems, activity dependent intrinsic properties play important roles in regulating rhythms [19]. Given this, we wondered whether larval motor neurons display any activity-dependent intrinsic properties that operate on times scales similar to the cycle periods seen during crawling rhythms.

Motor neurons display long lasting AHPs following volleys of action potentials. Figure 1a shows an overall schematic of the larval preparation (top) and a close view of the ventral ganglion showing motor neuron orientations and designations (bottom). Figure 1b shows a whole cell patch recording from motor neuron MNISN-Is (nomenclature of Hoang and Chiba, 2001). In response to a 5 sec, 100 pA current injection, the neuron fires action

potentials robustly. Afterwards, the membrane potential hyperpolarizes by ~20 mV and then takes 15–20 sec to return to baseline. Smaller, but still apparent AHPs are also visible through a range of shorter, 1 sec current pulses (Fig. 1c). After confirming that AHPs were observed in all dorsal motor neurons previously characterized (data not shown), we focused our work primarily on two identified motor neurons, MNISN-Is and MN30-Ib.

Membrane currents underlying the AHP

What intrinsic membrane currents underlie the observed AHP in larval motor neurons? First, we asked if the AHP was stimulated by spiking of the neuron or by membrane depolarization alone. We measured AHPs, then blocked voltage-gated sodium channels by applying 10^{-6} M tetrodotoxin (TTX). Figure 1d shows the response of a single neuron to a 5 sec, 100 pA current injection in control conditions (left) and in TTX (right). In TTX, the neuron does not spike and shows no AHP, even though levels of membrane depolarization are comparable to control. Mean membrane potentials at various time points after a volley of stimuli for pooled data from 5 preparations are shown at the right ($P<0.05$ at 2, 10, and 15 sec after stimulus end, Student's T-test). Note that after a 100 pA pulse, the AHP persists for over 10 sec in control conditions.

In a number of systems, AHPs are the result of Ca^{2+}-dependent potassium currents[20]. *Drosophila* larval motor neuron AHPs, however, do not require external Ca^{2+}, because they can be observed with Ca^{2+}-free saline and low free calcium (ca. 10^{-8} M) intracellular solutions (Figure 1). TTX experiments suggested that the current underlying the AHP was dependent on Na^+ influx into the motor neurons. Na^+-dependent K^+ channels have been shown to underlie long lasting AHPs in other organisms [21], [22]. We reasoned that if a K^+ conductance were responsible, then there would be a decrease in input resistance during the AHP. To test this, we estimated input resistance by injecting small hyperpolarizing current pulses before and during AHPs. Figure 2a shows a motor neuron (MNISN-Is) response to a 5 sec, 100 pA current pulse followed by three 1 sec, −10 pA pulses during the AHP. We injected hyperpolarizing pulses at 1 sec, ~6 sec, and ~20 sec after the depolarizing pulse stopped. Note that the amplitude of the membrane response to hyperpolarizing current pulses is the same at all time points. We used these data to estimate input resistance before and during AHPs. Pooled data from these experiments (Fig. 2b) suggests that resting membrane input resistance does not change during the AHP, especially at peak amplitude (1 sec after pulse; $F = 0.99$, One-way ANOVA). Input resistance can vary as a function of holding potential; to control for this, we measured input resistance at hyperpolarizing potentials that spanned the voltages seen during AHPs. Response to hyperpolarizing pulses was linear through this range ($n = 5$; data not shown). These data suggest that a large change in membrane conductance (i.e. K^+ channel opening) does not underlie the AHP.

If AHPs are mediated by a K^+ current, then they should reverse at the predicted reversal for K^+ ions (−107 mV in our recording conditions). To look for AHP reversal, we depolarized cells to the same level from different, hyperpolarized holding potentials approaching −107 mV. Figure 2c shows AHP responses to 5 sec depolarizing current pulses at rest, and at three hyperpolarized holding potentials (−70, −80, −90 mV) in a MNISN-Is cell. Injected current was calibrated to bring the neuron to approximately the same level of depolarization,

regardless of holding potential. In this preparation, and in the pooled data (Fig. 2d), we saw no change in AHP amplitudes as a function of holding potential (F-value = 0.97, One-way ANOVA). Neurons quickly became unhealthy when held below −90 mV, so we were unable to measure AHP amplitude exactly at K^+ reversal potential. However, we were able to span a large range of hyperpolarized holding potentials with this approach, and we saw no hint of AHP reversal.

The above results are not consistent with the larval AHP being mediated by a K^+ current, but are consistent with classic features of Na^+/K^+ pump-mediated currents [23]. We therefore bath applied ouabain, a blocker of Na^+/K^+ ATPase, and measured the effect on AHP amplitude. Figure 2e shows a motor neuron (MNISN-Is) response to a 5 sec, 100 pA current injection in control saline (left) and in saline containing 10^{-4} M ouabain (right). In control conditions, a 5 sec, 100 pA pulse evokes a long lasting AHP. When the same cell is held at a similar membrane potential in ouabain, and given the same depolarizing pulse, no AHP is visible. Pooled data are shown in Figure 2f; AHP amplitude is plotted as a function of injected current. The AHPs evoked by both 1 sec and 5 sec pulses are abolished in ouabain ($P<0.05$ for 40–100 pA with 5 sec pulses, $P<0.05$ for 60–100 pA with 1 sec pulses, Student's T-test). This was not an indirect affect due to diminished spiking in ouabain; at all current injection levels except one (5 sec, 100 pA), the number of evoked spikes in control saline was less than the number of spikes in ouabain (Supplemental Table 1). Consistent with this being a manipulation of pump activity, we saw no significant changes in input resistance between control and experimental conditions (Fig. 2g; $P = 0.55$, Student's T-test).

Genetic inhibition of Na^+/K^+ pump function abolishes AHPs

Current clamp and pharmacology experiments suggested that Na^+/K^+ pump activity underlies long lasting AHPs in *Drosophila* motor neurons. To further confirm this, we used the *GAL4-UAS* system [24] to genetically manipulate Na^+/K^+ pump function. Previous work has shown that ectopic expression of a mutant (D369N) $Na/^+K^+$ ATPase alpha subunit can have dominant negative effects on pump function [25]. We drove expression of dnATPase in motor neurons using the *GAL4* driver *C380+GFP* (see methods), then quantified the effect this had on AHP amplitudes. Figure 3a shows motor neuron recordings from two genetic controls (*UAS-dnATPase/+* and *C380+GFP/+*, left and center) and from an animal expressing dnATPase in motor neurons (*C380+GFP/+; dnATPase/+*, right). Large AHPs are visible in both control traces, but not in the neuron expressing dnATPase. Pooled data for these experiments are shown in Figure 3b–d. After both 1 sec and 5 sec pulses, AHPs in motor neurons expressing dnATPase were severely attenuated when compared to controls (Fig. 3b; 1 sec pulses: $P<0.05$ for 120 pA, both controls; $P<0.05$ for 100 pA, GAL4 control; $P>0.05$ for all other current injection levels. 5 sec pulses: $P<0.05$ for 80–120 pA, GAL4 control; $P>0.05$ for all other current injection levels. One-way ANOVA with Tukey HSD posthoc test). As with the ouabain application, input resistance was not significantly different from controls (Fig. 3c; $P>0.05$, One-way ANOVA, Tukey HSD posthoc test). Resting membrane potential showed a non-significant trend to be more depolarized in neurons expressing the dominant negative ATPase (Fig. 3d; F-value = 0.07, One-way ANOVA).

While dnATPase-expressing neurons did not have a statistically significant increase in resting membrane potential, inhibiting pump function with dnATPase did have an effect on how cells responded to current injection. Supplemental Figure 1 shows spike frequency plotted as a function of 1 sec pulses of current in control animals and in cells expressing dnATPase in motor neurons. At most current injection levels (40–80 pA), experimental animals responded significantly more robustly to current injection ($P<0.05$, One-way ANOVA, Tukey HSD posthoc test). We did not attempt to control the resting membrane potential in these experiments, so the observed increase in excitability may be due in part to the slightly more depolarized membrane potential in dnATPase expressing cells.

To examine the functional consequences of manipulating Na^+/K^+ ATPase activity in MNs, we used a combination of GAL4/GAL80 drivers to drive dnATPase in MNs alone (see Methods). Animals expressing dnATPase in motor neurons crawled significantly slower than controls (Figure 4a; $P<0.05$, One-way ANOVA, Tukey HSD posthoc test). This decrease in speed reflects a decrease in the frequency of forward peristalsis (Fig. 4b; $P<0.05$, One-way ANOVA, Tukey HSD posthoc test), but not in direction change or backward peristalsis (Figs. 4c, d $P>0.05$, One-way ANOVA, Tukey HSD posthoc test for both.

AHPs are proportional to spike number regardless of activity pattern

Current clamp recordings, pharmacology, and genetic manipulation all demonstrate that AHPs in larval motor neurons are mediated by the activity of the Na^+/K^+ pump. Pump-mediated AHPs are directly linked to spiking in motor neurons, but are not strongly influenced by the membrane potential of the neuron. As a result, AHPs are uniquely positioned to act as a cellular sensor tuned solely to spiking and changes in intracellular sodium. Furthermore, because of their long time scale, AHPs could also be used to integrate spike number regardless of the activity pattern of the neuron. To test these ideas, we compared AHPs produced by different types of activity patterns. Figure 5a shows a MN30-Ib response to a 5 sec, 20 pA depolarization (left) and the same cell responding to a 5 sec train of 1 Hz, 0.5 sec, 40 pA current pulses (right). AHP amplitudes increased with increasing current injection in both situations (Fig. 5b). Interestingly, AHP amplitude was proportional to total spike number regardless of whether the cell was constantly active or bursting (Fig. 5c). A similar effect was observed in MNISN-Is cells: AHP amplitudes were proportional to spike number regardless of whether the cell was constantly activated for 1 sec or constantly activated for 5 sec (Figs. 5d and e). These data indicate that this AHP functions as a pattern-independent spike counter on the timescale of the endogenous motor rhythm.

AHPs modulate a K^+ conductance in motor neurons

Besides acting as a spike integrator, what other functional role does the AHP play in a rhythmically active neural circuit? Because larval motor neurons are rhythmically active during crawling, they provided a unique opportunity to explore this question. In a second set of experiments, we gave rhythmic current injections to larval motor neurons designed to mimic the kind of synaptic input that they would receive during crawling. Previous studies of *Drosophila* larvae have shown that the cycle period of a typical stride (i.e. one full tail to head, peristaltic wave) is ~1 sec [15], [16]. To approximate endogenous crawling activity, we

gave trains of 20, 0.5 sec long bursts at a frequency of 1 Hz and at various current injection strengths. We measured spiking activity and membrane potentials during troughs in between bursts and after rhythmic trains. Figure 6a shows a MN30-Ib cell response to rhythmic 40 pA current injections. Note that after the first burst, a small AHP is generated, slightly hyperpolarizing the cell after the burst. This AHP is compounded after each burst until it reaches a steady state after ~5 cycles.

Figure 6b shows expanded time scale views of the 1st, 5th and 20th bursts in the train shown in **6a**. Note that as the trough potential between bursts hyperpolarizes, the spiking pattern of the neuron changes. There is no delay to 1st spike in the initial burst, whereas in later bursts there is a substantial delay. Figure 6c shows delay to first spike plotted as a function of cycle number for two current injection levels (40 pA, 100 pA). In both cases, the delay to first spike increases and reaches steady state after ~5 cycles. At all current injection levels, there was a significantly longer delay to first spike by the end of the rhythmic train (Fig. 6d; $P < 0.05$, Student's T-test). As cycle number increased, the longer delays to first spike were accompanied by a significant hyperpolarization of trough potentials (Fig. 6e). Spike rate did not significantly change (Fig. 6f). When these hyperpolarizations were cancelled out with depolarizing current injection, delays to first spike within bursts immediately shortened, returning to durations comparable to those seen in leading bursts (n = 5, data not shown), indicating that the change in duration is mediated by the AHP.

Previous work [18] has shown that delays to first spike in larval motor neurons are mediated by the *Shal*-encoded I_A current (I_{shal}). Furthermore, Ib type motor neurons have I_{shal} channels that are largely inactivated at resting V_m (ca. −55 mV in a silent cell). The AHP-mediated hyperpolarizations seen during rhythmic trains move the trough potential into a voltage range that would release I_{shal} from inactivation and cause a delay to first spike.

Activity-dependent AHPs interacted with I_{shal} to modify motor neuron intrinsic properties during rhythmic bouts. However, AHPs also interacted with I_{shal} even in the absence of rhythmic inputs if there was a history of activity. Figure 7a shows MN30-Ib voltage traces during the last two cycles of a rhythmic train of twenty 40 pA pulses (left) and responses to depolarizing current injection at 3 times after the train stopped (right). For 7–8 sec after the end of a rhythmic bout, the cell remains hyperpolarized. For several seconds following a train, if the cell is depolarized above spiking threshold, a clear delay to first spike is visible. Even though there are no rhythms, the motor neuron intrinsic properties are being held in a state mimicking what they would be doing during rhythmic activity by the actions of the AHP. Figure 7b shows the average delay to first spike at the 1st, 5th and 20th bursts in a train of 20 depolarizing inputs; it also shows average delay to first spike in bursts at 2.5, 5, and 10 seconds after the train has ended. For up to 5 seconds following the train, delay to first spike remains significantly longer than the delay seen in the first burst of the train ($P < 0.05$, one-way ANOVA with Tukey HSD).

DISCUSSION

One of the most important tasks of a neuron is to keep track of its own activity. This is of obvious importance for neurons that are involved in memory processes, but it is also true for

many other types of neurons that need to operate within a particular activity or input-output range. Many types of plasticity mechanisms have been described that allow cells to adjust synaptic weights and intrinsic properties to reflect their activity history and maintain optimal functionality. In this study, we demonstrate a new form of short-term cellular memory in *Drosophila* larval motor neurons that is mediated by spike-dependent activation of Na^+/K^+-ATPase. We show that an AHP mediated by electrogenic activity of the Na^+/K^+ pump is proportional to the number of proceeding spikes, even when the pattern of activity is varied. This AHP effectively acts as a spike counter at behaviorally relevant spike rates. Furthermore, we find that this AHP can release endogenous I_{shal} channels from inactivation during rhythmic firing, and that this modification persists for multiple seconds in the absence of rhythmic input, providing a memory trace of the rhythmically active state.

Na^+/K^+ pumps are commonly portrayed as the necessary but unglamorous workhorses of neuronal membranes. By continually moving Na^+ ions out and K^+ ions into cells, Na^+/K^+ pumps generate an electrochemical gradient across the cellular membrane; this slow activity is crucial for generating the resting membrane potential in all neurons and setting basal excitability. Na^+/K^+ pumps can have other functions, however. Long lasting, Na^+/K^+ pump-mediated AHPs have been observed in a variety of neuronal types. In *Drosophila* they have been shown to be engaged by pharmacological manipulation of sodium channel inactivation kinetics [26]. In various vertebrate preparations, pump-mediated AHPs regulate rhythmic bursting [27], [28] by suppressing excitability. Pump-mediated AHPs have also been shown to underlie changes in the efficacy of neuromodulatory synaptic input in leech sensory neurons [29]. This same pump current has been shown to be intimately involved in sensory coding in these neurons due to its ability to allow adaptive scaling of input signals[30]. To our knowledge, the present study is the first to show that a persistent (many seconds long), dynamic change in neuronal excitability can be attributed to Na^+/K^+ pump function under normal physiological conditions in rhythmically active motor neurons.

AHPs as spike counters and cellular memory mechanisms

One striking feature of the AHP reported here is that it reflects overall previous spiking activity but remains relatively insensitive to the pattern of activity in which spikes are presented. This is not a feature of the long lasting AHPs which are mediated by ionic conductances [31]. Spike counting has been shown to underlie memory formation in other systems. In weakly electric fish, a long-lasting shift in intrinsic excitability is responsible for a pulse integrating mechanism that is immune to frequency-dependent fluctuations. This process is critical to a form of long lasting sensorimotor adaptation in electric organ discharges [32].

The role of spike counting in the mature larval locomotor circuit is less clear, but the ability of AHPs to act as spike integrators or ‘spike counters’ through a range of activity patterns has interesting implications for computational neuroscientists interested in homeostatic plasticity. In previous work, models of how neurons keep track of their own activity have been focused on sensors of intracellular Ca^{2+} [3]. Intracellular Ca^{2+} levels, however, are not always well correlated with spiking activity in neurons [33]. Furthermore, Ca^{2+}-sensing mechanisms that operate on time scales over 1 sec are sometimes difficult to justify in a

model, given the fast time constant of Ca^{2+} decay after spiking (typically ~0.5 sec; [5]). Intracellular Na^+ concentrations, by contrast, are more directly linked to spiking since they directly reflect the actions of voltage-gated Na^+ channels. Our work, and that of others [9, 10] suggests that activity can modify intracellular Na^+ levels over multi-second time scales. Such accumulation is likely to be most significant in small neurons or geometrically constrained subcellular compartments. These results suggest that activity sensors tuned to intracellular Na^+ could be potentially useful as seconds-long time scale activity integrators in computational models of homeostatic plasticity. This has special relevance to rhythmic networks since many of these circuits operate with cycle periods of this magnitude.

An additional interesting property of the hyperpolarization produced by the larval pump is that it can release endogenous I_{shal} channels from inactivation and thereby modify how a cell responds to the next depolarizing input. Previous studies in the larval motor circuit concluded that I_{shal} currents are largely inactivated at rest and do not affect spike timing in MN30-Ib cells [18]. This conclusion, however, was based on measurements from silent cells. This is not the usual state of MN30-Ib cells; in a behaving animal, MN30-Ibs are rhythmically active. The importance of considering a network's endogenous activity in studies of synaptic plasticity has been demonstrated in other systems [34]. The example shown here highlights the importance of considering the endogenous activity of a network when measuring intrinsic properties in neurons as well. The ability of the AHP to alter the intrinsic properties of motor neurons embedded in the firing locomotor circuit marks them as having been recently active and alters the timing of motor outputs.

Role of the larval AHP in network output

The extent to which activity-dependent intrinsic properties can lead to forms of cellular memory has been widely studied [35–39]. However, putting these phenomena in a functional context is often difficult. Genetic inhibition of Na^+/K^+ ATPase activity in motor neurons abolishes AHPs. This genetic manipulation clearly has an impact on network output: it slows forward peristalsis by reducing CPG cycle period (Fig. 4). One possibility is that normal AHPs facilitate proper segment-to-segment coordination by restricting the time-frame of rhythmic activity within a segment during a peristaltic wave. When this restriction is removed (as in the case when dnATPase is expressed in motor neurons), activity is 'slurred' over a longer time frame in each segment, potentially leading to longer overall peristaltic wave durations. Tight control of activity bursts has been shown to be an important factor in regulating cycle period in other segmentally coupled oscillating networks [40, 41]. At this time, we do not have enough information about synaptic connectivity within the ventral ganglion to test this and other hypotheses using computational techniques, however, future work could address this question as circuit information becomes available.

It is important to note that in addition to abolishing AHPs, expression of dnATPase also affects motor neuron response to current injection. As a result, some of the behavior effects seen could be caused by hyperexcitation. Unfortunately, currently available genetic tools do not allow us to manipulate AHP amplitude and response to current injection independently. However, the dnATPase manipulation does not significantly affect resting membrane potential (Fig. 3D); in addition, the behavioral effects of acutely depolarizing motor neurons

with the heat-activated ion channel dTRPA1 (i.e. full stop, no peristalsis, [42]) are different from those reported in this study. These observations suggest that the pump-mediated affects on CPG output observed here are not merely the result of massive motor neuron depolarization. Overall, our results suggest that the seconds-long time scale of AHPs could act to keep motor neuron properties primed for rhythmic action and provide a complement to the longer term plasticity processes that engage translational and transcriptional mechanisms [43] to tune intrinsic properties in this circuit.

METHODS

Transgenic lines and growth conditions

For whole cell patch measurements of Na^+/K^+ pump mediated AHPs, we used animals in which a *GAL4* driver (*C380-GAL4*) known to express in motor neurons was recombined with *UAS-mCD8-GFP*, then outcrossed to wild type *Canton S (+/+)* animals (full genotype: *C380-GAL4, UAS-mCD8-GFP; +/+; +/+; +/+*. Abbreviation: *C380+GFP*). Expression of GFP was used to target neurons for recording. To inhibit Na^+/K^+ pump function in motor neurons, we crossed homozygous *C380+GFP* flies to *UAS-D369N* (full genotype: *+/+; +/+; UAS-D369N; +/+*. Abbreviation: *UAS-dnATPase*). This construct drives expression of an alpha subunit of the Na^+/K^+ pump with a point mutation in a highly conserved region of the ATPase. Previous work has shown that this construct acts as a partial dominant negative on Na^+/K^+ ATPase function [25].

For behavior experiments, we limited expression of dnATPase to motor neurons alone by using *C380+GFP* combined with *Cha-GAL80* (Full genotype: *C380-GAL4, UAS-mCD8-GFP/+;Cha-GAL80/+; UAS-D369N/+; +/+*. The addition of the *GAL80* gene inhibits *GAL4* expression in cholinergic sensory neurons (data not shown) and limits expression primarily to motor neurons [42]. All fly lines were grown on standard medium at 23–25°C on a roughly 12h:12h LD cycle.

Whole cell patch electrophysiology

All experiments were performed on female 3rd instar larvae. For physiology experiments, larvae were dissected in a modified 'A' physiological saline containing 128 mM NaCl, 2 mM NaOH, 2 mM KCl, 0 mM$CaCl_2$, 15 mM sucrose, 5 mM Trehalose, 4 mM $MgCl_2$, and 5 mM HEPES, with pH 7.1–7.2 [18]. First, each larva was pinned down in a sylgard-lined dish. A longitudinal incision was made along the dorsum and then the animal was filleted out by pinning down the body wall. Sheath tissue surrounding dorsal motor neuron clusters was digested with 0.01% protease (type XIV, Sigma, St. Louis, MO, www.sigmaaldrich.com) as previously described [18]. Motor neurons MNISN-Is (embryonic identity: RP2) and MN30-Ib (embryonic identity: RP1 or RP4) were targeted for recording [18, 44]. Pipette resistances were 5–10 MΩ. The internal pipette solution contained 130 mM potassium gluconate, 10 mM HEPES, 1 mM EGTA, 2 mM $MgCl_2$, 0.1 mM $CaCl_2$, 2 mM NaCl, 10 mM KOH, with pH adjusted to 7.2 with KOH. This composition results in a free calcium level on the order of 1.2×10^{-8} M in the intracellular solution.

During recordings, we used a gravity fed perfusion system to constantly superfuse preparations with saline. We performed all electrophysiology in 0.0 mM or 0.3 mM $CaCl_2$. No differences were observed between the two solutions (data not shown). Experiments involving rhythmic stimulations designed to mimic behaviorally relevant depolarizations were done in saline containing $CaCl_2$. In some experiments, we washed either 10^{-6} M tetrodotoxin (TTX) or 10^{-4} M ouabain (both from Sigma), over preparations using custom built perfusion switching valves.

We used MP285 micromanipulators (Sutter Instruments, Novato, CA, www.sutter.com) to maneuver patch electrodes, an Axopatch 200B to perform whole cell recordings, and a Powerlab 4/30 (ADinstruments, Colorado Springs, CA, www.adinstruments.com) combined with Chart 5.1 (ADinstruments) to record voltage traces on a Dell desktop PC. Data were analyzed using Spike2 (version 5, Cambridge Electronic Design, Cambridge, UK, www.ced.co.uk) and Excel (Microsoft, Redmond, WA, www.microsoft.com). Spike2 analysis scripts are freely available at http://www.whitney.ufl.edu/BucherLab.

Behavior

To measure larval locomotion parameters, we washed 3rd instar females in deionized water (to remove excess food), then allowed them to acclimate on dishes filled with 1% Bacto agar dissolved in de-ionized water for 15–20 min. 5–10 individuals at a time were transferred into a 25 × 25 cm arena also filled with 1% agar. After waiting ~1 min, we filmed crawling for a further 1 min using a VL3-ZU digital camcorder (Sharp electronics, Mahwah, NJ, www.sharpusa.com). A light box was placed under the arena to enhance contrast. Movies were recording using Windows Movie Maker on a desktop PC. Larval crawling speed and direction change were calculated with Dynamic Image Analysis (DIAS, http://keck.biology.uiowa.edu/) software. Statistical tests were performed in Excel and JMP.

Statistical analysis and data presentation

We performed statistical tests for both electrophysiological and behavioral studies in Excel and JMP (version 5, JMP, Cary, NC, www.jmp.com). Final figures were made in Canvas 9 (Deneba, Victoria, Ca).

Supplementary Material

Refer to Web version on PubMed Central for supplementary material.

Acknowledgments

This work was supported by National Institutes of Health grant R01 MH067284 to L. C. Griffith. We would like to thank Eve Marder, Barry Trimmer, and Paul Miller for helpful discussions and critical reading of the manuscript.

References

1. Cavazzini M, Bliss T, Emptage N. Ca^{2+} and synaptic plasticity. Cell Calcium. 2005; 38:355–367. [PubMed: 16154476]
2. Cudmore RH, Turrigiano GG. Long-term potentiation of intrinsic excitability in LV visual cortical neurons. J Neurophysiol. 2004; 92:341–348. [PubMed: 14973317]

3. Liu Z, Golowasch J, Marder E, Abbott LF. A model neuron with activity-dependent conductances regulated by multiple calcium sensors. J Neurosci. 1998; 18:2309–2320. [PubMed: 9502792]
4. Turrigiano G, Abbott LF, Marder E. Activity-dependent changes in the intrinsic properties of cultured neurons. Science. 1994; 264:974–977. [PubMed: 8178157]
5. Koch, C. Biophysics of Computation. Oxford University Press; Oxford: 1999.
6. Chaudhuri D, et al. Alternative splicing as a molecular switch for Ca^{2+}/calmodulin-dependent facilitation of P/Q-type Ca^{2+} channels. J Neurosci. 2004; 24:6334–6342. [PubMed: 15254089]
7. Canepari M, Vogt KE. Dendritic spike saturation of endogenous calcium buffer and induction of postsynaptic cerebellar LTP. PLoS ONE. 2008; 3:e4011. [PubMed: 19104665]
8. Canepari M, Vogt K, Zecevic D. Combining voltage and calcium imaging from neuronal dendrites. Cell Mol Neurobiol. 2008; 28:1079–1093. [PubMed: 18500551]
9. Rose CR. Na^+ signals at central synapses. Neuroscientist. 2002; 8:532–539. [PubMed: 12467375]
10. Bhattacharjee A, Kaczmarek LK. For K^+ channels, Na^+ is the new Ca^{2+} Trends Neurosci. 2005; 28:422–428. [PubMed: 15979166]
11. Richter DW. Generation and maintenance of the respiratory rhythm. J Exp Biol. 1982; 100:93–107. [PubMed: 6757372]
12. Rossignol S, et al. Plasticity of locomotor sensorimotor interactions after peripheral and/or spinal lesions. Brain Res Rev. 2008; 57:228–240. [PubMed: 17822774]
13. Marder E, Bucher D. Understanding circuit dynamics using the stomatogastric nervous system of lobsters and crabs. Annu Rev Physiol. 2007; 69:291–316. [PubMed: 17009928]
14. Stent GS, et al. Neuronal generation of the leech swimming movement. Science. 1978; 200:1348–1357. [PubMed: 663615]
15. Saraswati S, Fox LE, Soll DR, Wu CF. Tyramine and octopamine have opposite effects on the locomotion of *Drosophila* larvae. J Neurobiol. 2004; 58:425–441. [PubMed: 14978721]
16. Fox LE, Soll DR, Wu CF. Coordination and modulation of locomotion pattern generators in *Drosophila* larvae: effects of altered biogenic amine levels by the tyramine beta hydroxlyase mutation. J Neurosci. 2006; 26:1486–1498. [PubMed: 16452672]
17. Cattaert D, Birman S. Blockade of the central generator of locomotor rhythm by noncompetitive NMDA receptor antagonists in *Drosophila* larvae. J Neurobiol. 2001; 48:58–73. [PubMed: 11391649]
18. Choi JC, Park D, Griffith LC. Electrophysiological and morphological characterization of identified motor neurons in the *Drosophila* third instar larva central nervous system. J Neurophysiol. 2004; 91:2353–2365. [PubMed: 14695352]
19. McCormick DA, Pape HC. Properties of a hyperpolarization-activated cation current and its role in rhythmic oscillation in thalamic relay neurones. J Physiol. 1990; 431:291–318. [PubMed: 1712843]
20. Pedarzani P, Stocker M. Molecular and cellular basis of small--and intermediate-conductance, calcium-activated potassium channel function in the brain. Cell Mol Life Sci. 2008; 65:3196–3217. [PubMed: 18597044]
21. Kim U, McCormick DA. Functional and ionic properties of a slow afterhyperpolarization in ferret perigeniculate neurons *in vitro*. J Neurophysiol. 1998; 80:1222–1235. [PubMed: 9744934]
22. Sanchez-Vives MV, Nowak LG, McCormick DA. Cellular mechanisms of long-lasting adaptation in visual cortical neurons *in vitro*. J Neurosci. 2000; 20:4286–4299. [PubMed: 10818164]
23. Catarsi S, Scuri R, Brunelli M. Cyclic AMP mediates inhibition of the Na(+)-K+ electrogenic pump by serotonin in tactile sensory neurones of the leech. J Physiol. 1993; 462:229–242. [PubMed: 7687293]
24. Brand AH, Perrimon N. Targeted gene expression as a means of altering cell fates and generating dominant phenotypes. Development. 1993; 118:401–415. [PubMed: 8223268]
25. Sun B, Xu P, Wang W, Salvaterra PM. *In vivo* modification of Na^+/K^+ ATPase activity in *Drosophila*. Comp Biochem Physiol B Biochem Mol Biol. 2001; 130:521–536. [PubMed: 11691629]

26. Wu Y, Cao G, Pavlicek B, Luo X, Nitabach MN. Phase coupling of a circadian neuropeptide with rest/activity rhythms detected using a membrane-tethered spider toxin. PLoS Biol. 2008; 6:e273. [PubMed: 18986214]
27. Rozzo A, Ballerini L, Abbate G, Nistri A. Experimental and modeling studies of novel bursts induced by blocking Na^+ pump and synaptic inhibition in the rat spinal cord. J Neurophysiol. 2002; 88:676–691. [PubMed: 12163521]
28. Johnson SW, Seutin V, North RA. Burst firing in dopamine neurons induced by N-methyl-D-aspartate: role of electrogenic sodium pump. Science. 1992; 258:665–667. [PubMed: 1329209]
29. Scuri R, Lombardo P, Cataldo E, Ristori C, Brunelli M. Inhibition of Na^+/K^+ ATPase potentiates synaptic transmission in tactile sensory neurons of the leech. Eur J Neurosci. 2007; 25:159–167. [PubMed: 17241277]
30. Arganda S, Guantes R, de Polavieja GG. Sodium pumps adapt spike bursting to stimulus statistics. Nat Neurosci. 2007; 10:1467–1473. [PubMed: 17906619]
31. Wallen P, et al. Sodium-dependent potassium channels of a Slack-like subtype contribute to the slow afterhyperpolarization in lamprey spinal neurons. J Physiol. 2007; 585:75–90. [PubMed: 17884929]
32. Oestreich J, Dembrow NC, George AA, Zakon HH. A “sample-and-hold” pulse-counting integrator as a mechanism for graded memory underlying sensorimotor adaptation. Neuron. 2006; 49:577–588. [PubMed: 16476666]
33. Darbon P, Pignier C, Niggli E, Streit J. Involvement of calcium in rhythmic activity induced by disinhibition in cultured spinal cord networks. J Neurophysiol. 2002; 88:1461–1468. [PubMed: 12205166]
34. Pulver SR, Bucher D, Simon DJ, Marder E. Constant amplitude of postsynaptic responses for single presynaptic action potentials but not bursting input during growth of an identified neuromuscular junction in the lobster, *Homarus americanus*. J Neurobiol. 2005; 62:47–61. [PubMed: 15389685]
35. Marder E, Abbott LF, Turrigiano GG, Liu Z, Golowasch J. Memory from the dynamics of intrinsic membrane currents. Proc Natl Acad Sci U S A. 1996; 93:13481–13486. [PubMed: 8942960]
36. Turrigiano GG, Marder E, Abbott LF. Cellular short-term memory from a slow potassium conductance. J Neurophysiol. 1996; 75:963–966. [PubMed: 8714669]
37. Winograd M, Destexhe A, Sanchez-Vives MV. Hyperpolarization-activated graded persistent activity in the prefrontal cortex. Proc Natl Acad Sci U S A. 2008; 105:7298–7303. [PubMed: 18474856]
38. Heyward P, Ennis M, Keller A, Shipley MT. Membrane bistability in olfactory bulb mitral cells. J Neurosci. 2001; 21:5311–5320. [PubMed: 11438607]
39. Koh HY, Weiss KR. Activity-dependent peptidergic modulation of the plateau-generating neuron B64 in the feeding network of *Aplysia*. J Neurophysiol. 2007; 97:1862–1867. [PubMed: 17202238]
40. Masino MA, Calabrese RL. A functional asymmetry in the Leech Heartbeat Timing Network is revealed by driving the network across various cycle periods. J Neurosci. 2002; 22:4418–4427. [PubMed: 12040049]
41. McClellan AD, Hagevik A. Coordination of spinal locomotor activity in the lamprey: long-distance coupling of spinal oscillators. Exp Brain Res. 1999; 126:93–108. [PubMed: 10333010]
42. Pulver SR, Pashkovski SL, Hornstein NJ, Garrity PA, Griffith LC. Temporal dynamics of neuronal activation by Channelrhodopsin-2 and TRPA1 determine behavioral output in *Drosophila* larvae. J Neurophysiol. 2009
43. Baines RA, Uhler JP, Thompson A, Sweeney ST, Bate M. Altered electrical properties in *Drosophila* neurons developing without synaptic transmission. J Neurosci. 2001; 21:1523–1531. [PubMed: 11222642]
44. Hoang B, Chiba A. Single-cell analysis of *Drosophila* larval neuromuscular synapses. Dev Biol. 2001; 229:55–70. [PubMed: 11133154]

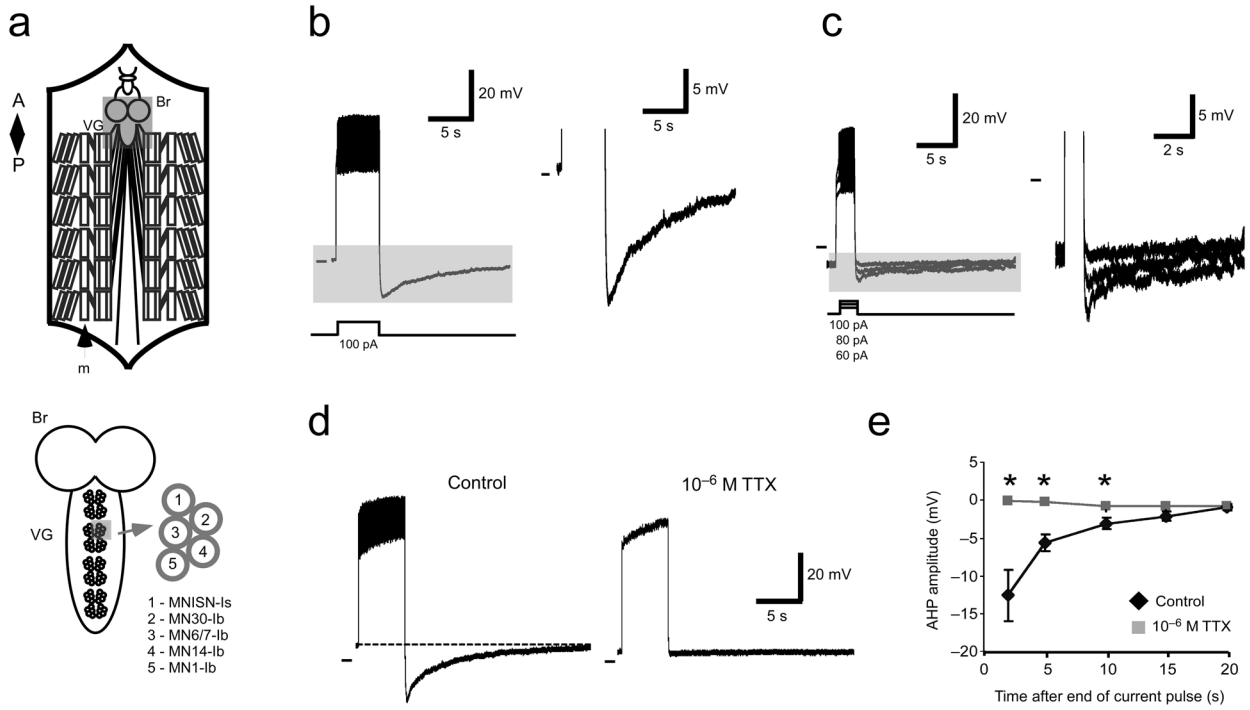

Figure 1.

Dorsal motor neurons in 3rd instar larvae show a long lasting Na^+-dependent AHP following volleys of action potentials. **a)** Schematic of the larval preparation (top) showing brain (Br), ventral ganglion (VG) and body wall muscles (m). Below, close view of dorsal motor neuron orientations and designations. **b)** Response to a 5 sec, 100 pA current injection. Shaded area is shown at right. **c)** Response to 1 sec current pulses (different preparation). Increasing the current injection amplitude increases the peak hyperpolarization reached. Shaded area is shown at right. **d)** TTX abolishes AHPs. Left, MNISN-Is response to 5 sec, 100 pA current pulses in control (left) and **10^{-6}** M TTX (right). Right, pooled data. Asterisks indicate significant differences between control and TTX responses ($P<0.05$, Student's T-test). Pooled data are presented as mean ± SEM.

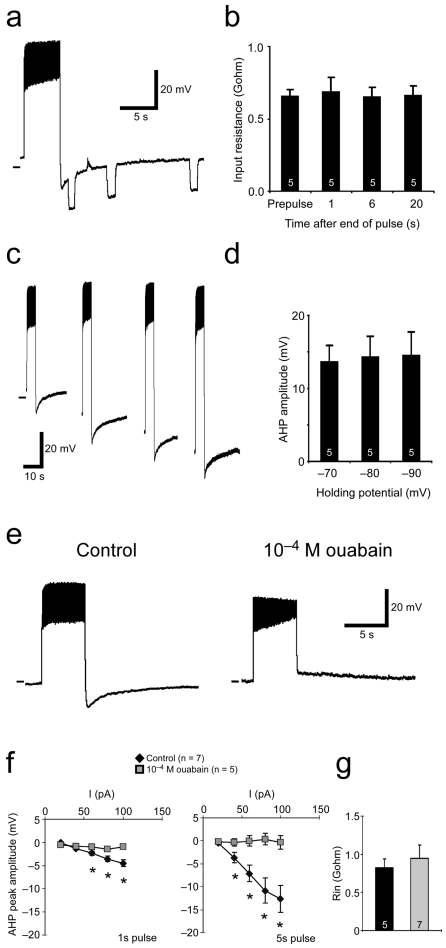

Figure 2.

The larval AHP shows electrophysiological and pharmacological features of a Na^+/K^+ pump current. **a)** Input resistance does not change during AHPs. Left, motor neuron response to a 5 sec, 100 pA current pulse followed by 1 sec, −5 pA pulses at 3 time points during the AHP. **b)** Pooled data from experiments shown in **a**. Input resistance was estimated from single hyperpolarizing current pulses before spiking (prepulse) and at 1, 6, and 20 sec after spiking ceased. No significant differences were observed among the time points ($P>0.05$, One-way ANOVA). **c)** AHPs do not show signs of reversing at the predicted reversal for K^+ ions. Left, motor neuron responses to 5 sec current pulses at 4 different holding potentials. At each holding potential, cell is depolarized to approximately the same level. **d)** Pooled data for hyperpolarized holding potentials. No significant differences in AHP amplitude were observed at the various holding potentials ($P>0.05$, One-way ANOVA). **e)** Recordings from a motor neuron in control saline (left) and in ouabain (right). In ouabain, hyperpolarizing current has been injected to hold the resting potential at control levels. **f)** AHP amplitudes plotted as a function of injected current in control conditions (black diamonds) and in ouabain (grey squares). AHPs are almost completely abolished after both 1 and 5 sec current pulses. Asterisks indicate significant differences between control and ouabain responses ($P<0.05$, Student's T-test). **g)** Input resistances in control and ouabain

were not significantly different (P>0.05, Student's T-test). Pooled data are presented as mean ± SEM. Sample size is indicated on histogram bars.

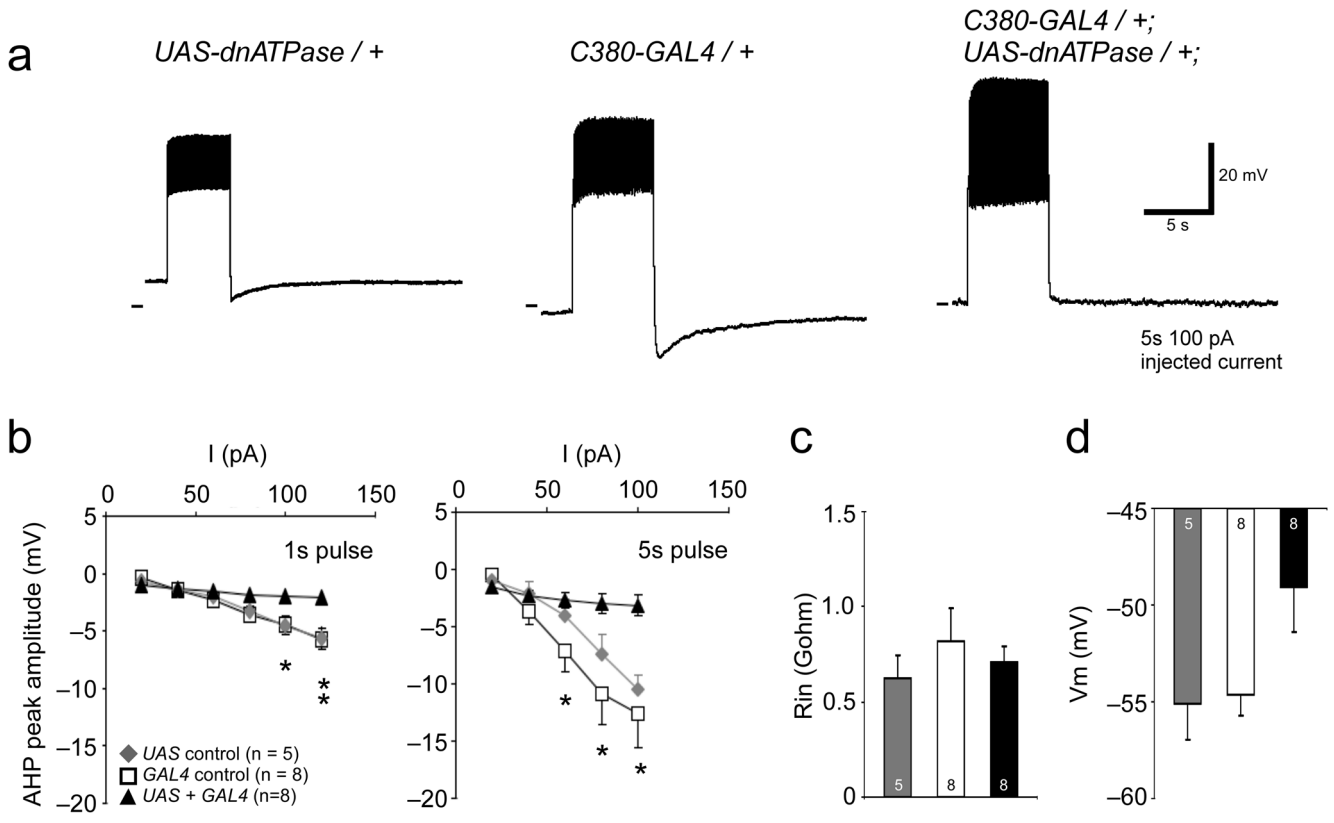

Figure 3.

Expression of dominant negative Na^+/K^+ ATPase decreases AHP amplitude in motor neurons. **a)** Representative recordings from motor neurons in *UAS* control (left) and *GAL4* control (center) and *GAL4* + *UAS* larvae (right). Note lack of AHP in experimental conditions **b)** AHP amplitude plotted as a function of injected current in control conditions (squares and diamonds) and in flies expressing dnATPase (triangles). Asterisks indicate significant difference between dnATPase data ($P<0.05$, One-way ANOVA with Tukey HSD posthoc test). **c)** Input resistances were the same in control and experimental animals ($P>0.05$, One-way ANOVA with Tukey HSD posthoc test). **d)** Resting membrane potential was slightly depolarized in dnATPase expressing cells (F-value = 0.07. All pooled data are shown as mean ± SEM.

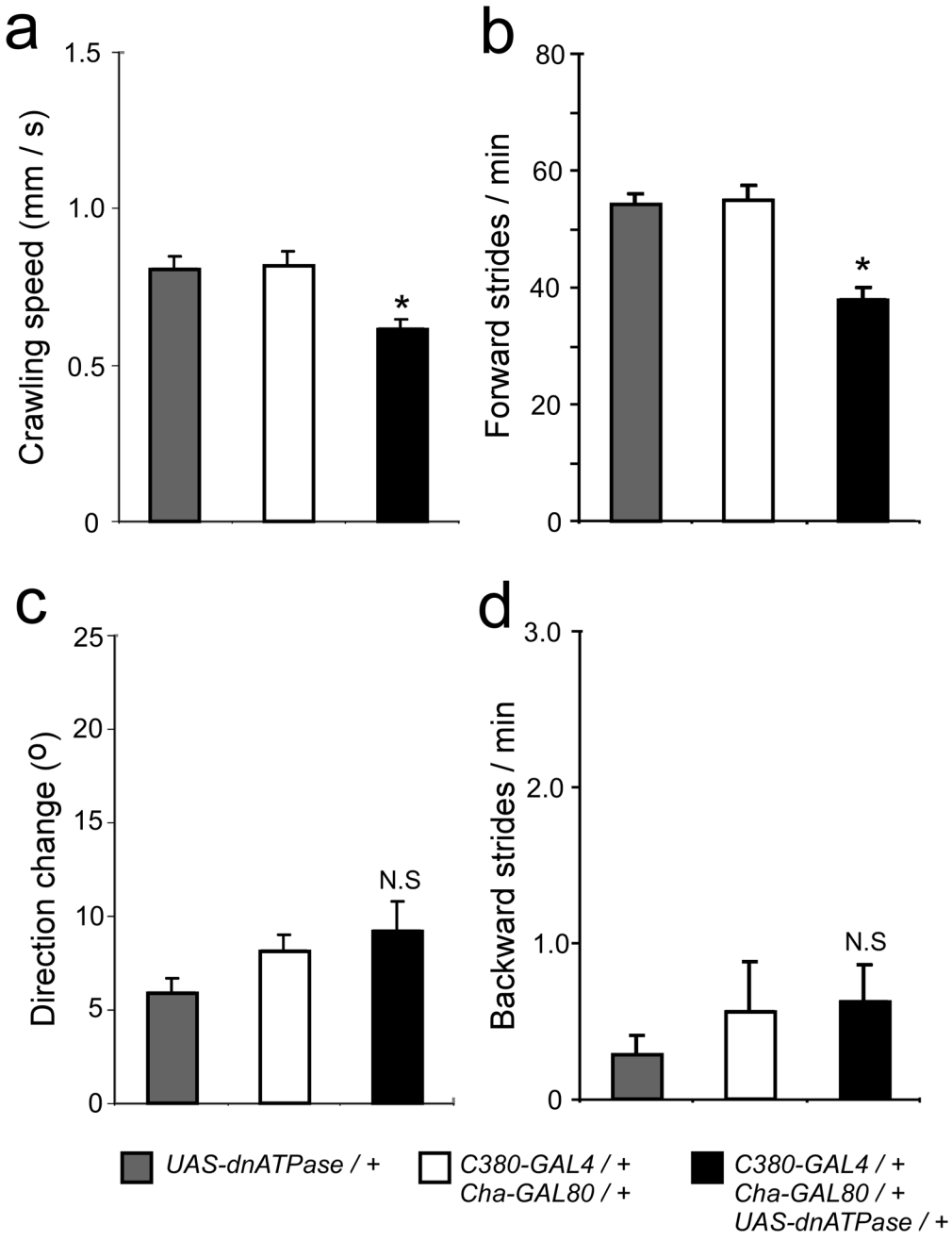

Figure 4.

Expressing dnATPase in motor neurons decreases the cycle period of network output. **(a)** Animals expressing dnATPase in motor neurons crawl slower than controls. **(b)** Direction change during crawling is not altered by dnATPase expression. **(c)** The frequency of forward peristalsis is reduced in animals expressing dnATPase. **(d)** The frequency of backwards peristalsis is unaffected by dnATPase expression. Asterisks indicate significant differences from controls ((P<0.05, One-way ANOVA, Tukey HSD posthoc test). All pooled data are shown as mean ± SEM.

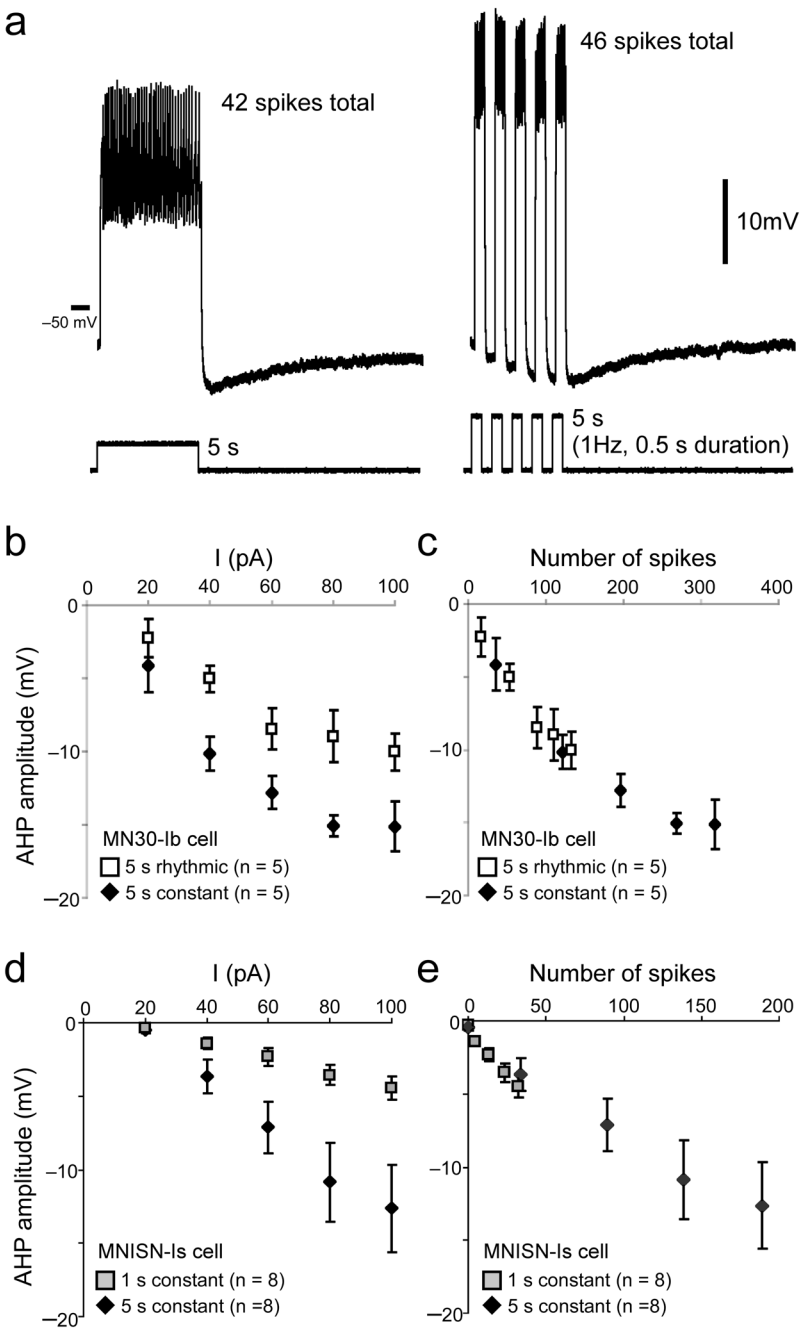

Figure 5.

AHP amplitude is proportional to spike number regardless of activity pattern. **a)** MN30-Ib cell response to a 5 sec, 20 pA depolarization (left), and 5 sec of 40 pA rhythmic depolarizations (1 Hz, 0.5 sec duration) (right). **b)** AHP amplitude in MN30-Ib cells at various current injection levels for the two stimulus patterns. **c)** AHP amplitude as a function of total spike number after constant and rhythmic stimuli. **d, e)** MNISN-Is cell AHPs after 1 sec and 5 sec constant pulses. All pooled data are presented as mean ± SEM.

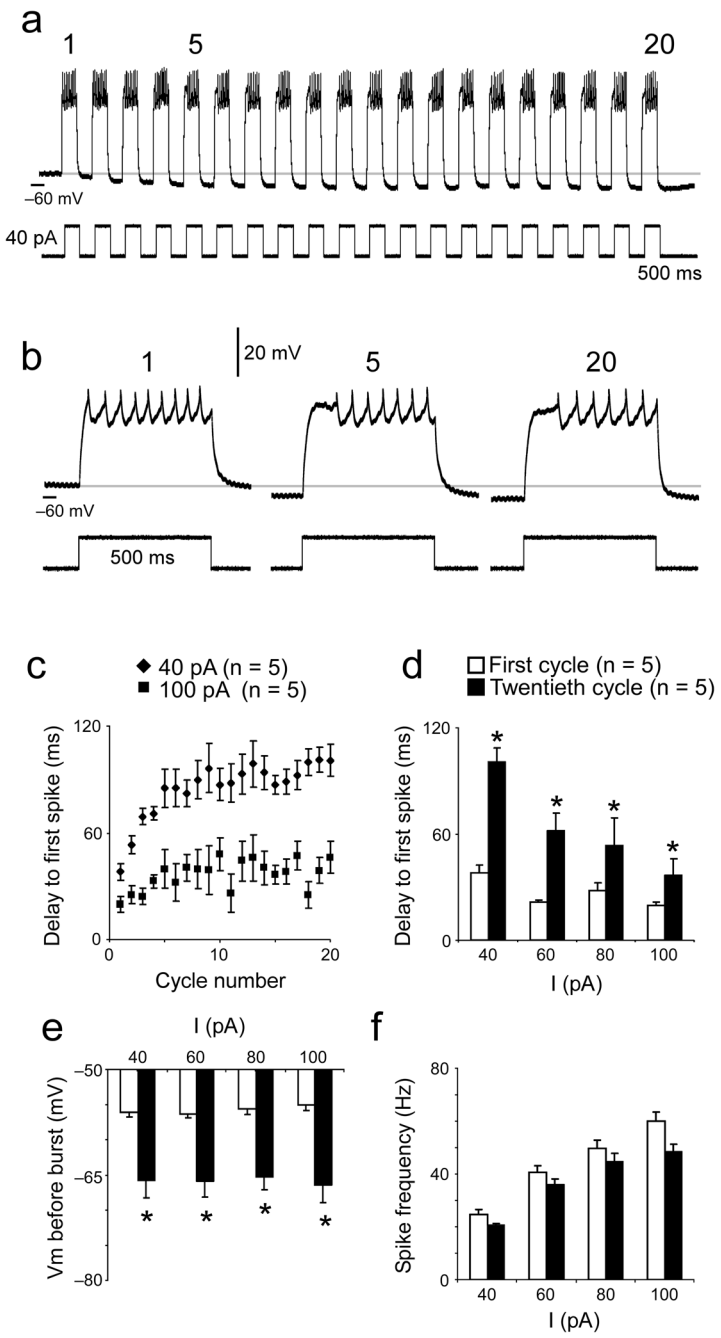

Figure 6.

AHPs release *Shal*-type I_A channels from inactivation and modify motor neuron intrinsic properties during behaviorally relevant rhythmic depolarization. **a)** MN30-Ib response to a train of depolarizing stimuli (40 pA, 1Hz, 0.5 sec duration). **b)** Close views of bursts 1, 5, and 20. Note delay to first spike in later cycles. Gray line denotes initial resting membrane potential. **c)** Delay to first spike plotted as a function of cycle number for two levels of current injection. **d)** Initial and final delay to first spike for 4 levels of current injection. **e)** Membrane potential before initial and final bursts at various current injection levels. **f)** Spike

frequency within initial and final bursts at various current injection levels. All pooled data are presented as mean ± SEM. Asterisks indicate P<0.05, Student's T-test.

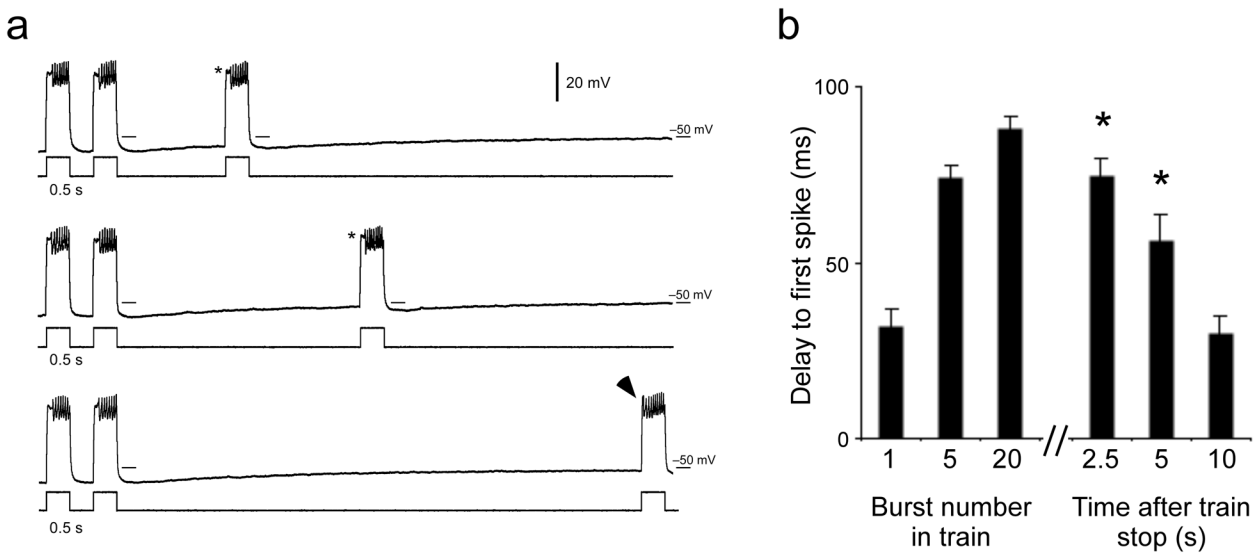

Figure 7.

AHPs are able to hold intrinsic properties in states approximating those seen during rhythmic activity even in the absence of rhythmic inputs. **a)** MN30-Ib cell responses to 40 pA current injections at various times following a 20 sec train of rhythmic depolarizing stimuli (40 pA, 1Hz, 0.5 sec duration). Last two bursts of the train are shown at left. The delay to first spike at the end of the train persists for multiple seconds (asterisks) even though the cell is not being driven rhythmically. As V_m returns to rest, the delay to first spike is lost (arrowhead). **b)** Average delay to first spike in the 1^{st}, 5^{th} and 20^{th} bursts of a train, followed by average delays at 2.5, 5, 10 sec after cessation of train. Asterisks indicate times at which delay to first spike is significantly longer than 1^{st} burst ($P < 0.05$, One-way ANOVA, with Tukey HSD posthoc test). All pooled data are shown as mean ± SEM.